

# Preparation and Corrosion Resistance of $\gamma$ -aminopropyltriethoxysilane-TiO<sub>2</sub>-GO/Waterborne Polyurethane Coating

Xia Wang\*, Xiong Li, Ling-long Xu, Qiao Zhang, Yue Gu

School of Material Science and Engineering, Southwest Petroleum University, Chengdu 610500, People's Republic of China

\*E-mail: [lxiong088@163.com](mailto:lxiong088@163.com)

Received: 23 July 2020 / Accepted: 8 September 2020 / Published: 30 September 2020

---

In this paper,  $\gamma$ -aminopropyltriethoxysilane-TiO<sub>2</sub>-GO (KTG) composite particles were prepared using  $\gamma$ -aminopropyltriethoxysilane (KH550) by depositing nano-TiO<sub>2</sub> on graphene oxide (GO) substrate. The KTG/waterborne polyurethane (WPU) composite coating was prepared by blending KTG with WPU. Fourier transform infrared spectroscopy (FTIR), x-ray diffraction (XRD), and scanning electron microscope (SEM) were employed to characterize the composition and structure of the GO before and after the modification, while the water resistance, thermal stability and corrosion resistance of the composite coating were examined via water absorption test, contact angle test, thermogravimetric analysis (TGA), and electrochemical impedance spectroscopy (EIS). The results showed that nano-TiO<sub>2</sub> was successfully deposited on the GO surface. The incorporation of KTG composite particles reasonably improved the water resistance, thermal stability and corrosion resistance of the WPU coating. Optimum water resistance of the composite coating with 0.9% KTG incorporation, 1.3% water absorption rate reduction relative to the pure WPU coating, and 283 to 300°C increment in thermal decomposition temperature were achieved. Moreover, the corrosion resistance of the composite coating was significantly improved. Furthermore, a value of  $7.89 \times 10^6 \Omega \cdot \text{cm}^2$  coating resistance of the composite coating,  $2.56 \times 10^{-9} \text{ A} \cdot \text{cm}^{-2}$  corrosion current density, and 99.81% corrosion inhibition efficiency can be attained.

---

**Keywords:** graphene oxide; nano-TiO<sub>2</sub>; waterborne polyurethane; corrosion resistance

## 1. INTRODUCTION

Traditional solvent-based polyurethane coatings are a common and effective strategy for protecting steel structures from corrosion owing to their good physical barrier to water, oxygen, and corrosive ions[1]. However, during the preparation and application of solvent-based polyurethane coatings, a large amount of volatile organic compounds are released, resulting in environmental pollution

and waste of resources[2]. In recent years, with an increase in people's awareness of environmental protection, the application of solvent-based polyurethane coatings has been greatly limited, prompting the development of polyurethane coatings toward water-repellant, solvent-free, powdered and enhanced strength coating properties[3]. Among them, waterborne polyurethane (WPU) coating has become one of the research hotspots in the field of coatings due to its characteristics of safety, non-toxicity, good compatibility and substrate adhesion[4~6].

However, the hydrophilic groups in the WPU form polar channels, increasing the water absorption and permeability in the coating, and reducing the shielding property against water, oxygen and other corrosive media, thereby weakening the corrosion resistance of the WPU coating[7]. To solve this problem, inorganic nanoparticles have been employed as fillers to improve the water and corrosion resistances of WPU coatings. In recent years, the widespread application of graphene oxide (GO) as a filler in improving the water and corrosion resistances of WPU coatings has attracted significant attention[8]. GO is a special structure composed of carbon atoms in the two-dimensional honeycomb lattice of graphene and oxygen-containing functional groups such as hydroxyl groups, carboxyl groups, and epoxy groups on the sheet layer and along the edge layer. It has a strong shielding performance against corrosive media, which can improve the penetration resistance of the coating[9~11]. Cui[12] prepared nanocomposite coatings by blending functionalized GO with WPU and depositing them on galvanized steel sheets, thereby improving the metal's water and corrosion resistances. However, the active functional groups contained on the surface of the GO lead to its poor thermal stability, and studies have shown that modifying inorganic nanoparticles on the surface of GO is an innovative strategy for improving its thermal stability. This can not only increase the GO layer spacing and thermal stability but also prevents any potential agglomeration in the coating[13]. Presently, nanoparticles such as  $\text{SiO}_2$ [14],  $\text{TiO}_2$ [15],  $\text{Al}_3\text{O}_4$ [16],  $\text{CaCO}_3$ [17], and  $\text{Fe}_3\text{O}_4$ [18] are used to modify the surface property of GOs. Nano- $\text{TiO}_2$  is often used as a filler for polymer coatings due to its excellent weather and corrosion resistances, however it readily agglomerates leading to uneven dispersion in the polymer matrix and affects the performance of the composite. Wang[19] employed silane coupling agent KH550 in modifying nano- $\text{TiO}_2$ , and a successful grafting of the agent on the oxide surface was reported via FTIR and SEM analyses. The experimental results revealed that the modified nano- $\text{TiO}_2$  has better dispersion performance in WPU coating. Studies have shown that the organic modification of nano- $\text{TiO}_2$  can reduce its surface tension and improve its dispersion stability in a polymer matrix[20].

In this paper, the surface of nano- $\text{TiO}_2$  was modified using silane coupling agent KH550, and the introduced amino functional groups are combined with that of GO to prepare nano- $\text{TiO}_2$  and GO composite particles (KTG). A KTG/WPU composite coating with different incorporation amounts of GO was prepared by blending KTG with WPU. The water, heat, and corrosion resistances of KTG/WPU composite coatings were studied.

## 2. EXPERIMENT

### 2.1 Materials

Rutile nano- $\text{TiO}_2$  was provided by Shanghai Aladdin Biochemical Technology Co., Ltd. Waterborne polyurethane (WPU) was provided by Shenzhen Jitian Chemical Co., Ltd. Graphene oxide

(GO) and  $\gamma$ -aminopropyltriethoxysilane (KH550) as well as the anhydrous ethanol and hydrochloric acid used in this article were provided by Chengdu Kelong Chemical Reagent Factory.

## 2.2 Preparation of KTG

A certain amount of sodium hexametaphosphate dissolved in 50 ml of absolute ethanol and 2 g of nano-TiO<sub>2</sub> were uniformly mixed. The solution was evenly dispersed by a 750 r/min mixer and an ultrasonic disperser, and the pH was adjusted to 8, then an aqueous solution of silane coupling agent KH550 was slowly added while stirring at 80 °C. After 4 h of reaction, the mixture was centrifuged and filtered, then washed with absolute ethanol and deionized water. Finally, the washed mixture was dried and ground into a modified nano-TiO<sub>2</sub> powder (KT).

The KT and GO powders with a mass ratio of 1:3 were introduced into 100 mL of an organic solvent (N,N dimethylformamide), then ultrasonically dispersed for 30 min and stirred at 105 °C for 3 h. The product was then centrifuged, washed with absolute ethanol and deionized water, and dried at 60 °C for 24 h to obtain a modified GO sample (KTG).

## 2.3 Preparation of the KTG/WPU composite coating

KTG powder was added to the WPU emulsion in a certain proportion (the mass fractions of KTG were 0%, 0.5%, 0.7%, 0.9%, 1.2% and 1.5%). After 30 min of ultrasonic dispersion, mechanical stirring was continued for 1 h to obtain a KTG/WPU composite emulsion. Then, the composite emulsion was coated on the pretreated 304 stainless steel surface using a wire bar coater. Finally, the coating was cured at 60 °C for 48 h, and the thickness was 80±5 μm.

## 2.4 Characterization

Fourier transform infrared spectroscopy (FTIR) analysis of the GO particles before and after modification was performed using a Nicolet 6700. The KBr tablet method was used for the sample preparation and the test range was 500–4000 cm<sup>-1</sup>.

Thermogravimetry analysis (TGA) was performed using DSC823 TGA/SDTA85/e instrument to measure the thermal weight loss of the coating film sample. Under a nitrogen atmosphere, the thermal stability of the coating was analyzed from 40 to 600 °C at a temperature rise rate of 10 °C/min.

The contact angle was measured at 25 °C using a micro-syringe to obtain a static contact angle from 5 μl of water droplets on the coating surface. A contact angle goniometer (JGW-360A) was used to perform the measurement.

The sample was sealed with paraffin and the working area was 1 × 1 cm. The experimental instrument was a CS 310 electrochemical workstation and the corrosion medium was a 3.5% NaCl solution. The coated 304 stainless steel sample, saturated calomel electrode, and platinum electrode were employed as the working, reference, and auxiliary electrodes, respectively, in this three-electrode system. During the measurement of the electrochemical AC impedance, a sine wave with a voltage amplitude of 20 mV was applied to provide a disturbance. The frequency was in a range of 10<sup>-2</sup> to 10<sup>5</sup>

Hz. According to the polarization resistance value, the corrosion inhibition efficiency ( $\eta$ ) was calculated according to Eq. (1) as follows:

$$\eta(\%) = \frac{R_p - R_{p0}}{R_p} \times 100\% \tag{1}$$

where  $R_p$  and  $R_{p0}$  denote the polarization resistance of the KTG/WPU coating and bare steel, respectively.

A ZEISS EV0 MA15 scanning electron microscope (SEM) was used to analyze and observe the surface corrosion morphologies of the KTG/WPU composite coating samples that have been immersed in a 3.5% NaCl solution. The image magnification was 5000 $\times$  and the acceleration voltage was 20 kV.

### 3. RESULTS AND DISCUSSION

#### 3.1 Characterization of KTG

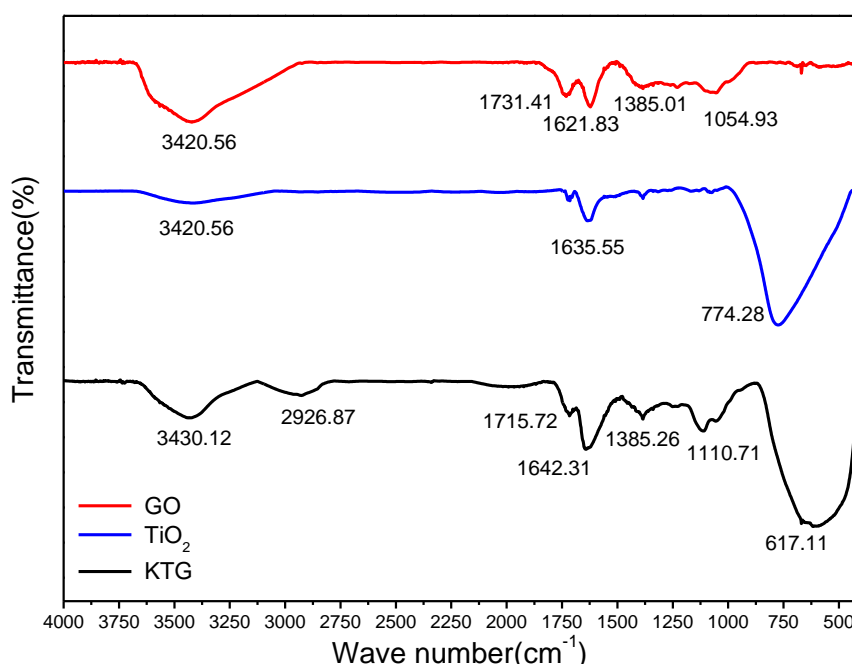


**Figure 1.** FTIR spectrum of the GO before and after modification

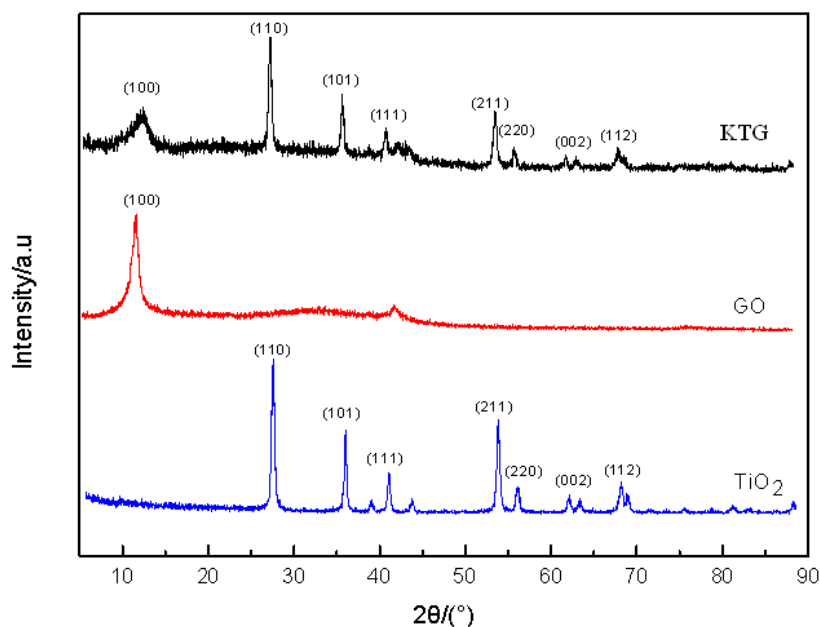


**Figure 2.** XRD of the GO before and after modification

As shown in Fig. 1, the absorption peaks of -OH, C=C and Ti-O-Ti of TiO<sub>2</sub> were observed at 3420.56 cm<sup>-1</sup>, 1635.55 cm<sup>-1</sup>, and 774.28 cm<sup>-1</sup>, respectively. The absorption peaks at 3420.56 cm<sup>-1</sup>, 1731.41 cm<sup>-1</sup>, 1621.83 cm<sup>-1</sup>, and 1054.93 cm<sup>-1</sup> were those of the -OH adsorbed on the GO surface, C=O stretching vibration in the carboxyl group, C=C stretching vibration of the benzene ring, and characteristic absorption peak of C-O-C[21]. The absorption peak of the infrared spectrum of KTG at 617.11 cm<sup>-1</sup> was consistent with the characteristic absorption peak of Ti-O-Ti of nano-TiO<sub>2</sub>, indicating that the KTG composite material contained the structure of nano-TiO<sub>2</sub>. The absorption peak at 2926.87 cm<sup>-1</sup> was the C-H tensile vibration peak in the -CH<sub>2</sub> modified group of KH550. The N-H bending vibration absorption peak appeared at 1642.31 cm<sup>-1</sup>, and the antisymmetric tensile vibration peak of Si-O-Si appeared at 1110.71 cm<sup>-1</sup>. The disappearance of C-O-C at 1054.93 cm<sup>-1</sup> indicated that the epoxy group of GO reacted with the amino group of KH550 coupling agent, confirming that the agent deposited the nano-TiO<sub>2</sub> successfully on the GO surface.

As shown in Fig. 2, the XRD spectrum of GO exhibited a sharp diffraction peak at about 11°, which is the characteristic diffraction peak of the oxide (100)[22]. In the XRD spectrum of KTG, the characteristic diffraction peak of nano-TiO<sub>2</sub> appeared, and the GO diffraction peak was still retained at about 11°, which indicated that the nano-TiO<sub>2</sub> was successfully deposited on the GO surface without destroying the GO structures.

### 3.2 Water resistance of the KTG/WPU composite coating

Water resistance is an important indicator to measure the anti-corrosion performance of coatings[23]. The water absorption properties of KTG/WPU composite coatings with different contents were analyzed by immersion weighing method. The water absorption of the KTG/WPU coating was calculated according to Eq. (2) as follows:

$$W(\%) = \frac{w_2 - w_1}{w_1} \times 100\% \tag{2}$$

where  $W_1$  denotes the initial mass of the coating and  $W_2$  represents the mass after soaking it for 24 h in a 3.5% NaCl solution.

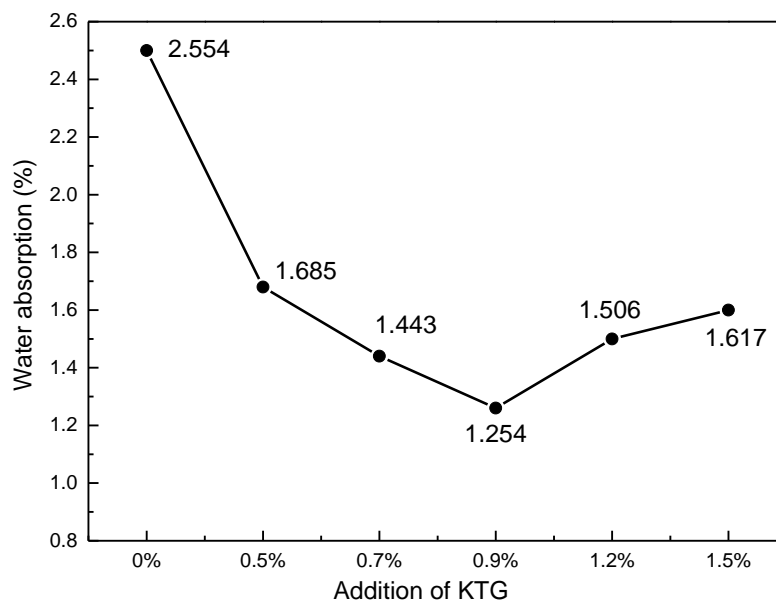


**Figure 3.** Effect of KTG addition on water absorption rate of the KTG/WPU coating

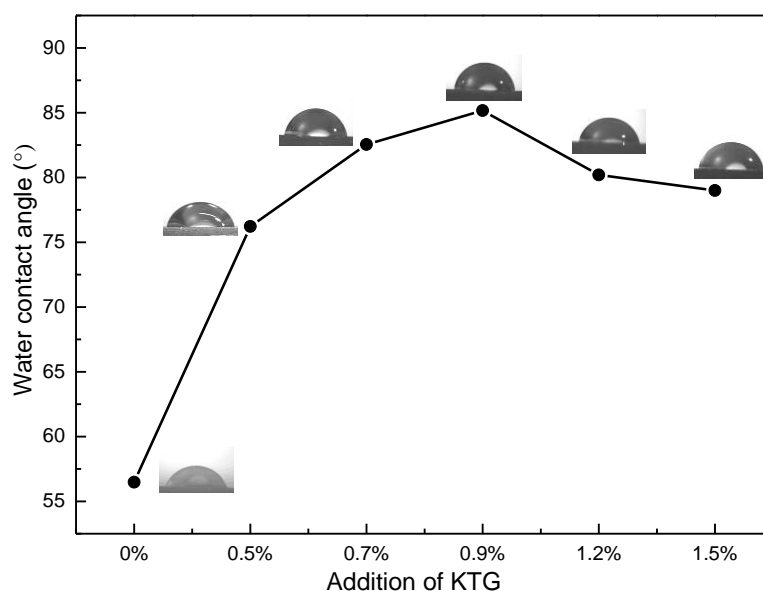


**Figure 4.** Effect of KTG addition on the hydrophobicity of the KTG/WPU coating

Since the surface of the GO sheet has a special structure composed of oxygen-containing functional groups such as hydroxyl, carboxyl, and epoxy, it has a strong shielding performance against corrosive media such as oxygen, water molecules, and chloride ions, thus the water resistance of the

coating can be improved using KTG composite particles as fillers. As shown in Figs. 3 and 4, compared with the pure WPU coating, the water absorption of the KTG/WPU composite coating and the water contact angle were significantly decreased and increased, respectively. Because KTG has a nanometer size, it can occupy the gaps of the WPU emulsion to prevent potential infiltration of corrosive ions. As the content of the KTG increased, the water absorption rate of the coating tends to stabilize. When the content exceeded 0.9%, the water absorption rate of the coating began to increase. The reason for this phenomenon is attributed to the uneven particle size distribution in the WPU coating resulting from excess KTG filler, which readily forms defects, thereby resulting in poor water resistance[24]. The water absorption rate of the composite coating with 0.9% KTG is 1.254% and the maximum water contact angle can reach 86°. This indicates that the WPU composite coating with a KTG content of 0.9% demonstrated the best water resistance.

### 3.3 Heat resistance of the KTG/WPU composite coating

The comparison between the pure WPU and KTG/WPU composite coatings via TGA analysis is shown in Fig. 5. The initial and final pyrolysis temperatures of the pure WPU coating were 240 °C and 432 °C, respectively, while the initial and final pyrolysis temperatures of the KTG/WPU composite coating were 257°C and 449 °C, respectively. The thermal decomposition temperatures of the pure WPU and KTG/WPU composite coatings at a weight loss rate of 5% were 283 and 300 °C, respectively, and the final residual amounts were 5.1% and 8.1%, respectively.

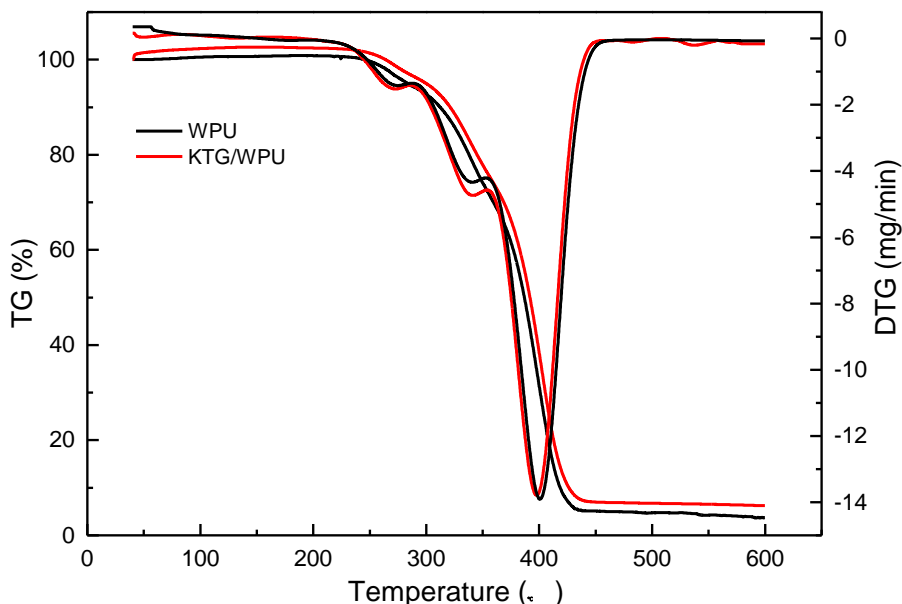


**Figure 5.** TGA curves of WPU coatings and KTG/WPU coatings

Compared with pure the WPU coating, the decomposition temperature of the KTG/WPU composite coating was increased by 17 °C and the decomposition rate was reduced by 3.0%. These data revealed that the thermal stability of the composite coating was improved after incorporating KTG particles. Similarly, Kale[25] also demonstrated that the thermal properties of WPU/GOSI films were

improved compared with pure WPU using graphene oxide-silica (GOSI) nanocomposites as fillers in the WPU coatings.

### 3.4 Corrosion resistance of the KTG/WPU composite coating

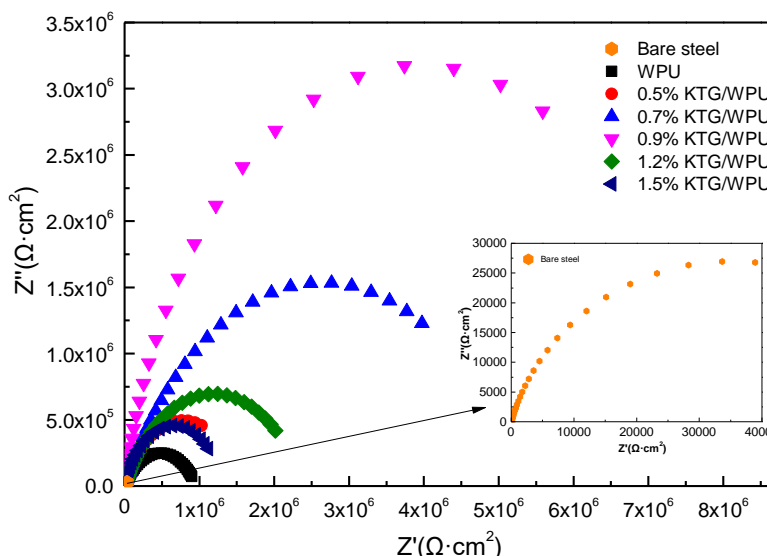


**Figure 6.** (a) Nyquist plots of different KTG content coatings after immersion in 3.5%NaCl solution for 12h

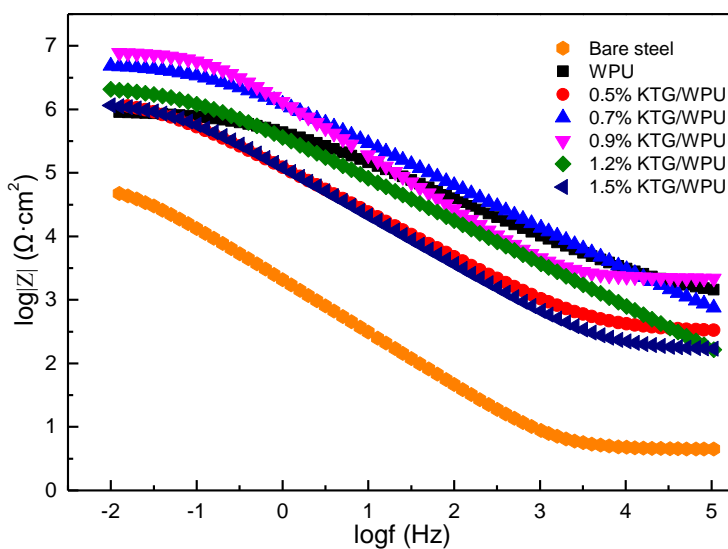


**Figure 6.** (b) Bode plots of different KTG content coatings after immersion in 3.5%NaCl solution for 12h

To determine the effect of KTG incorporation on the corrosion resistance of the coating, KTG/WPU composite coatings with different contents were prepared. An electron gap scanning (EIS) measurement was performed after immersing the coating in a 3.5% NaCl solution for 12 h. The

impedance spectra are shown in Fig. 6. It can be seen from Fig. 6(a) that the impedance arc radius of the KTG/WPU composite coating significantly outperformed that of the pure WPU coating. The results show that KTG inclusion can effectively improve the coating corrosion resistance. The arc resistance of the KTG/WPU composite coating increased first and then decreased with an increase in KTG amount. This is attributed to the KTG nanoparticles being able to fill the pores and gaps in the coating and improve the coating density, thereby enhancing its corrosion resistance. The resistance arc radius of the coating was largest when the amount of KTG added was 0.9%. However, when the content of KTG increased to 1.2% and 1.5%, the impedance arc radius of the composite coating significantly diminished and the corrosion resistance was weakened. This is attributed to excess entanglement and agglomeration of the KTG particles, resulting in uneven distribution. The particles formed void defects in the coating and corrosive ions easily infiltrate the substrate through the defect channel to corrode it. Cai[26] also realized that excessive integration of polyaniline/graphene (PANI/RGO) composite particles can lead to a significant deterioration in the shielding property when studying the anti-corrosion performance of the PANI/RGO composite anti-corrosion coatings. It can also be seen from Fig. 6(b) that when 0.9% KTG was integrated,  $\log(z)$  vs.  $\log(f)$  was a diagonal curve with a slope of 1, indicating that the coating at this time was equivalent to a barrier layer with a large resistance and small capacitance.

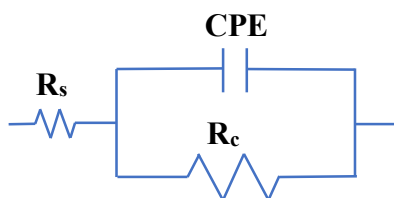


**Figure 7.** Equivalent circuit diagram of a KTG/WPU layer

**Table 1.** Data of  $R_s$  and  $R_c$  for different KTG content coatings by Nyquist plots fitting.

Sample	$R_s$ ( $\Omega \cdot \text{cm}^2$ )	CPE ( $\text{F} \cdot \text{cm}^{-2}$ )	$R_c$ ( $\Omega \cdot \text{cm}^2$ )
Bare steel	34.52	$1.04 \times 10^{-4}$	$7.04 \times 10^4$
WPU	41.61	$4.99 \times 10^{-6}$	$9.57 \times 10^5$
0.5% KTG/WPU	332.4	$2.10 \times 10^{-6}$	$1.52 \times 10^6$
0.7% KTG/WPU	244.0	$2.06 \times 10^{-8}$	$5.29 \times 10^6$
0.9% KTG/WPU	208.4	$1.10 \times 10^{-7}$	$7.89 \times 10^6$
1.2% KTG/WPU	298.3	$7.32 \times 10^{-7}$	$2.38 \times 10^6$
1.5% KTG/WPU	163.8	$1.92 \times 10^{-6}$	$1.31 \times 10^5$

The impedance data were fitted based on the equivalent circuit model shown in Fig. 7, and the impedance fitting parameters are shown in Table 1. In the figure,  $R_s$  represents the solution resistance. Since the same solution was adopted in each experiment and the difference between the solution and the

coating resistances was large,  $R_s$  can be ignored.  $R_c$  represents the coating resistance which reflects its electrolytes shielding ability and it is the main parameter used to evaluate the corrosion resistance. When the incorporated amount of KTG was 0.9%, the capacitance value of the WPU composite coating was  $1.10 \times 10^{-7} \text{ F}\cdot\text{cm}^{-2}$  and the maximum resistance value was  $7.89 \times 10^6 \text{ }\Omega\cdot\text{cm}^2$ . Thus, the WPU composite coating with a 0.9% KTG content offered the best corrosion resistance. The same EIS test revealed that the corrosion resistance of WPU coatings can be improved by incorporating nano-fillers. Wu[27] employed the sulfonated graphene/zinc phosphate (SG-ZP) composite material as the reinforcing material of the WPU-based composite coating, and the material effectively improved the corrosion resistance of the coating. The corrosion resistance is comparable to the experimental result obtained in this study.

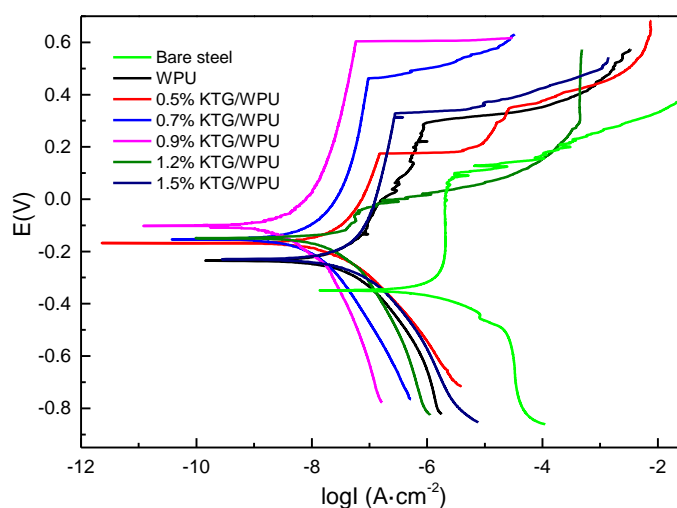


**Figure 8.** Polarization curves of coatings with different KTG contents after immersion in a 3.5% NaCl solution for 12 h

**Table 2.** Data of corrosion potential, corrosion current with corrosion rate for coatings with various KTG contents by polarization curve fitting

Sample	$E_{\text{corr}}$ (V)	$I_{\text{corr}}$ ( $\text{A}\cdot\text{cm}^{-2}$ )	Corrosion rate (mm/year)	$R_p$ ( $\Omega\cdot\text{cm}^{-2}$ )	$\eta$ (%)
Bare steel	-0.350	$1.12 \times 10^{-6}$	$1.32 \times 10^{-2}$	$2.32 \times 10^4$	—
WPU	-0.265	$2.82 \times 10^{-7}$	$3.40 \times 10^{-3}$	$1.28 \times 10^6$	98.18
0.5% KTG/WPU	-0.168	$1.35 \times 10^{-8}$	$1.58 \times 10^{-4}$	$1.94 \times 10^6$	98.80
0.7% KTG/WPU	-0.153	$4.74 \times 10^{-9}$	$5.57 \times 10^{-5}$	$5.51 \times 10^6$	99.58
0.9% KTG/WPU	-0.103	$2.56 \times 10^{-9}$	$2.54 \times 10^{-5}$	$1.21 \times 10^7$	99.81
1.2% KTG/WPU	-0.152	$2.01 \times 10^{-8}$	$2.36 \times 10^{-4}$	$1.30 \times 10^6$	98.22
1.5% KTG/WPU	-0.263	$8.20 \times 10^{-8}$	$9.65 \times 10^{-4}$	$3.18 \times 10^5$	92.70

As shown in Fig. 8, compared with the pure WPU coating, the polarization curve of the WPU composite coating with KTG was completely shifted to the upper left corner, the corrosion potential was increased, and the corrosion current density was lowered. The Tafel extrapolation method was used to fit the polarization curve, and the obtained curve parameters are shown in Table 2. As the KTG content increased, the corrosion current density first decreased and then increased, while the corrosion potential first increased and then decreased. The corrosion potential of the coating with 0.9% KTG was  $-0.103$  V, and the self-corrosion current density was  $2.56 \times 10^{-9}$  A·cm<sup>-2</sup>, which was two orders of magnitude lower than that of a pure WPU coating, the corrosion inhibition rate was increased from 98.18% to 99.81%. This shows that the WPU composite coating containing 0.9% KTG particles possessed the best corrosion resistance, which is consistent with the results obtained via impedance spectroscopy.

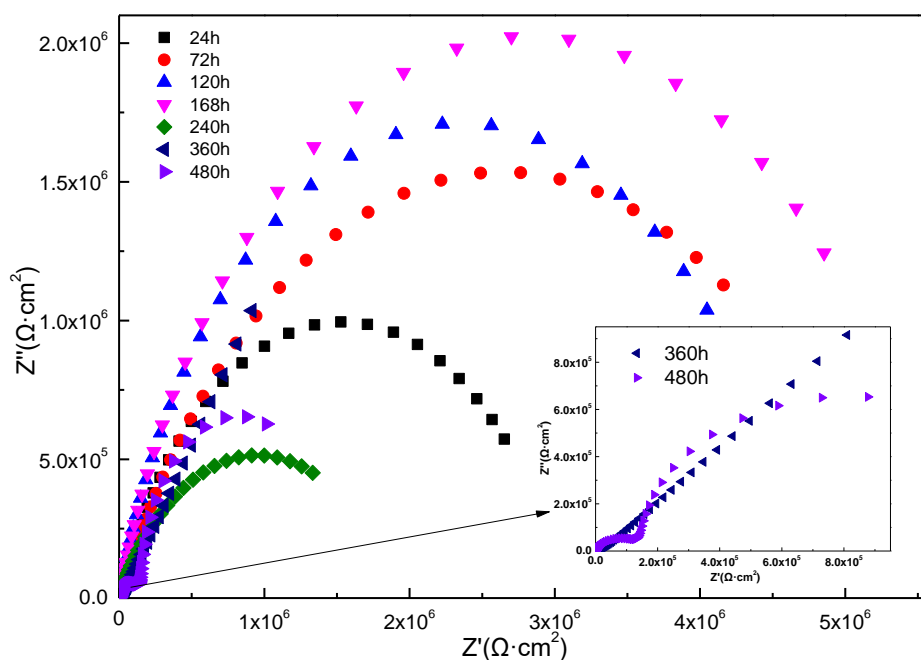


**Figure 9.** (a) Nyquist plots of KTG/WPU coatings after different immersion time in 3.5% NaCl

The WPU composite coating with 0.9% KTG was immersed in a 3.5% NaCl solution for a long time at 25 °C. The EIS test results are illustrated in Fig. 9. It can be seen from Fig. 9(a) that the impedance arc of the composite coating first increased and then decreased as the immersion time increased. The composite coating maintained a large impedance arc after immersion for 168 h. This was due to the uniform distribution of KTG nanoparticles in the coating, which improved the permeability of the coating and hinders the propagation of corrosive media[28].

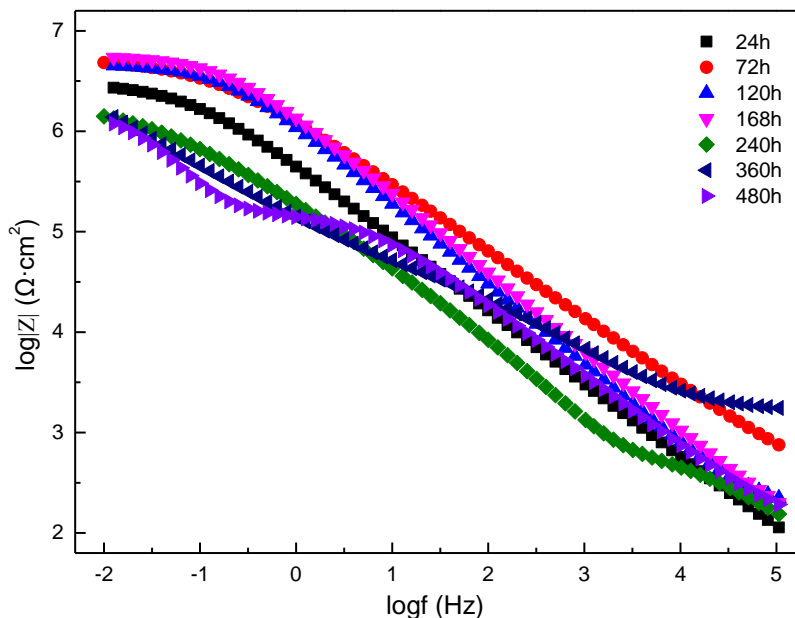


**Figure 9.** (b) Bode plots of KTG/WPU coatings after different immersion time in 3.5% NaCl

However, after immersion for 480 h, the impedance map exhibited an insignificant arc in the high-frequency region, indicating that the corrosive medium has infiltrated the substrate surface. It can be seen from Fig. 9(b) that the  $\log(z)$  vs.  $(f)$  curve shifted in the low-frequency direction as the immersion time increased. The impedance modulus continuously decreased, indicating that the penetration of the corrosive media resulted in decreased coating resistance.

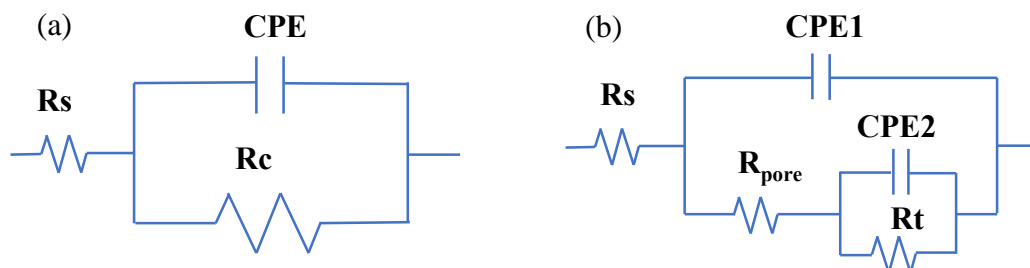


**Figure 10.** Equivalent circuit diagram of KTG/WPU at different soaking stages

Fig. 10 shows the employed equivalent circuit diagram for fitting the electrochemical impedance data for different immersion times. Figs. 10(a) and (b) present the equivalent circuit diagram at the initial and middle stages of immersion, respectively. In these figures,  $R_s$ ,  $R_c$ , and  $R_t$  represent the solution, coating, and charge-transfer resistances, respectively. Table 3 shows the electrochemical impedance parameters of the KTG/WPU coatings immersed for different times. After 72 h of immersion, the coating resistance can reach a value of  $5.29 \times 10^6 \Omega \cdot \text{cm}^2$ . This shows that a dense protective layer with a large resistance and low capacitance provided good protection to the base metal, indicating that the corrosive medium has not penetrated the coating at this time. When the immersion time increased to 168 h, the

coating resistance consequently increased to  $5.67 \times 10^6 \Omega \cdot \text{cm}^2$  but a charge transfer was initiated. This indicates that the corrosive medium began to penetrate the coating. However, the fitting data reflected higher coating resistance and lower capacitance, indicating that the coating still possesses a better corrosion protection effect. After immersing for 360 h, the  $R_t$  of the coating further increased and the coating resistance decreased to  $4.3 \times 10^4 \Omega \cdot \text{cm}^2$ .

**Table 3.**  $R_s$ ,  $R_c$ , and  $R_t$  for coatings with different KTG contents by Nyquist plot fitting

Soaking time	$R_s$ ( $\Omega \cdot \text{cm}^2$ )	CPE1 ( $\text{F} \cdot \text{cm}^{-2}$ )	$R_c$ ( $\Omega \cdot \text{cm}^2$ )	CPE2 ( $\text{F} \cdot \text{cm}^{-2}$ )	$R_t$ ( $\Omega \cdot \text{cm}^2$ )
24 h	85.6	$5.45 \times 10^{-8}$	$3.07 \times 10^6$	-	-
72 h	94.7	$2.06 \times 10^{-8}$	$5.29 \times 10^6$	-	-
120 h	159.1	$1.89 \times 10^{-7}$	$4.70 \times 10^6$	$2.49 \times 10^{-5}$	-
168 h	75.81	$1.56 \times 10^{-8}$	$5.67 \times 10^6$	$1.05 \times 10^{-6}$	$1.01 \times 10^3$
240 h	138.54	$9.05 \times 10^{-6}$	$4.16 \times 10^4$	$1.09 \times 10^{-5}$	$2.33 \times 10^4$
360 h	156	$5.55 \times 10^{-7}$	$4.30 \times 10^4$	$2.44 \times 10^{-6}$	$1.63 \times 10^{10}$
480 h	97.13	$4.95 \times 10^{-7}$	$1.66 \times 10^5$	$5.89 \times 10^{-7}$	$1.36 \times 10^6$

This is because the corrosive medium has penetrated the coating, decreasing the adhesion of the coating to the substrate[29]. Zhang[30] measured the adhesion strength of the WPU composite coating before and after 30 days of immersion in 3.5 wt.% NaCl solution. The results showed that the coating adhesion strength gradually decreased as immersion time increased, though the well-dispersed coating exhibited the least decrement. This indicates that an excellent dispersion ability of KTG is an important factor for composite coating, which enables a firmer adherence of the composite coating to the matrix, and effectively prevents the penetration of corrosive medium into the matrix[31], thus prolonging the adherence of the coating to the matrix surface[32]. When the immersion time was finally increased to 480 h, the corrosive medium completely penetrated the coating, leading to a barrier layer formed between the coating and substrate, eventually the metal substrate began to corrode.

To more intuitively investigate the morphological changes of the KTG/WPU coating during the corrosion process, coating samples with an immersion time of 0 h, 72 h, 168 h, and 360 h were selected for SEM observation at a magnification of 5000 $\times$ , as shown in Fig. 11. Compared with the KTG/WPU composite coating sample before immersion (Fig. 11(a)), it can be seen from Fig. 11(b) that after 72 h of immersion, a small number of protrusion occurred on the surface of the WPU composite coating.

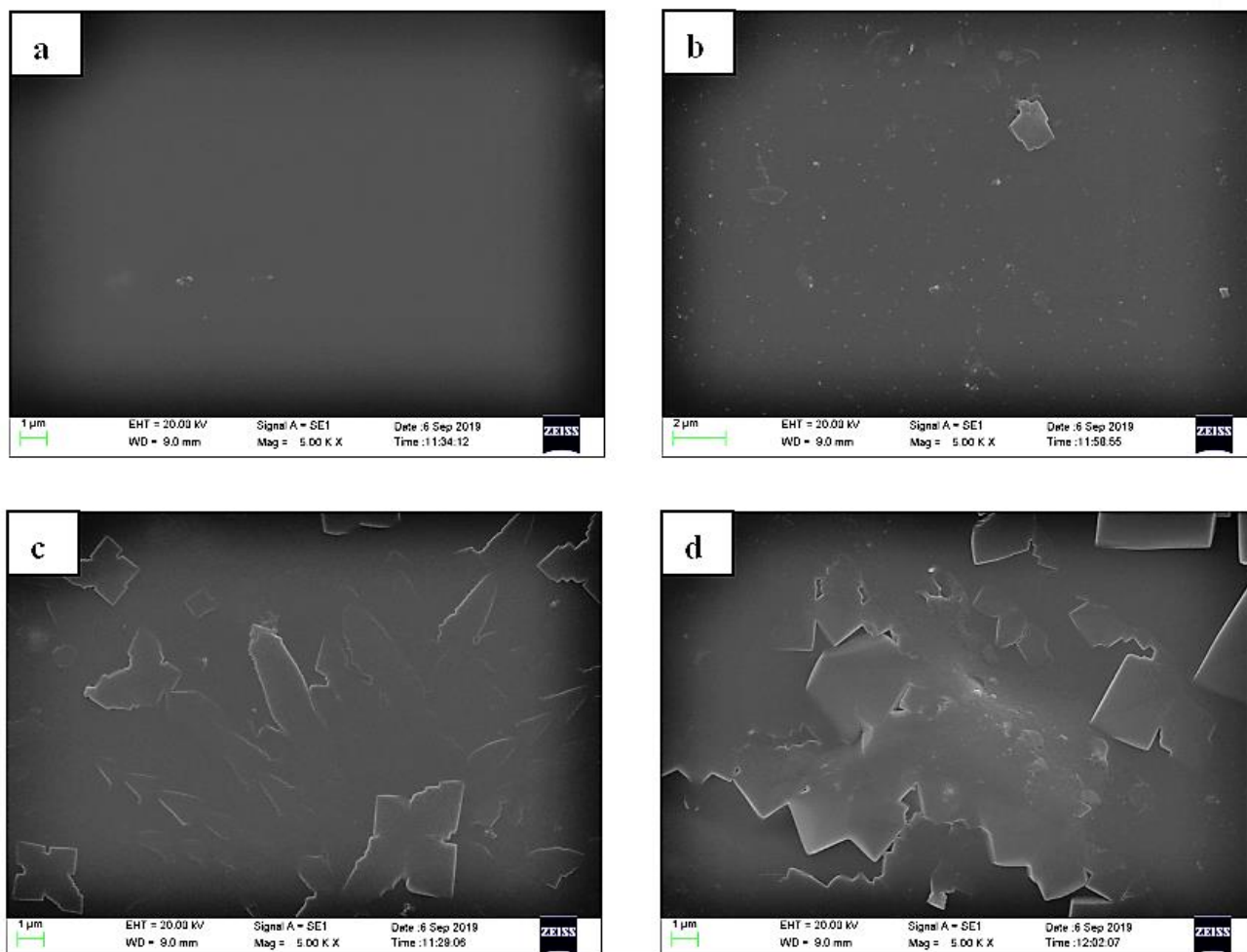


**Figure 11.** Scanning electron micrographs of KTG/WPU at different soaking stages

This indicated that a small amount of water molecules in the corrosive medium began to penetrate the coating, but the corrosive medium could not infiltrate the interface between the coating and metal substrate. Fig. 11(c) revealed that long edge lines appeared along the surface of the WPU composite coating after immersion for 168 h. This is because the corrosive medium penetrated the core of the composite coating from the edge of the KTG layer, resulting in blistering. Fig. 11(d) revealed that uneven and blocky protrusions appeared over the coating surface after immersion for 360 h, indicating that the water molecules in the WPU composite coating were close to saturation, and the corrosive medium has penetrated the interface between the coating and the metal substrate, resulting in decreased adhesion of the composite coating.

#### 4. CONCLUSION

(1) Compared with the pure WPU coating, the water absorption rate of the KTG/WPU composite coating immersed in 3.5% NaCl for 24 h was stable at 1.254%, and the water resistance significantly improved. Under the same condition, the water contact angle of the composite coating can

rise to 86°. The results showed that the KTG particles were uniformly dispersed in the WPU coating, which filled the voids in the composite coating, improving the compactness and water resistance of the coating.

(2) EIS and polarization curves showed that the resistance value of the WPU composite coating with a KTG content of 0.9% can reach  $7.89 \times 10^6 \Omega \cdot \text{cm}^2$  and the self-corrosion current density was  $2.56 \times 10^{-9} \text{ A} \cdot \text{cm}^{-2}$ , which exceeded two orders of magnitude less than that for the pure WPU coating. The corrosion inhibition rate reached 99.81%.

(3) The SEM image of the KTG/WPU composite coating showed that the effective protection time provided by the coating exceeded 168 h. The protective effect of the coating weakened with an increase in the immersion time, however, its anti-corrosive effect was retained even when the immersion time exceeded 360 h.

#### ACKNOWLEDGEMENTS

This work was supported by the National Natural Science Foundation of China (No.51774242)

#### References

1. R.B. Figueira, J.R. Silvac and E.V. Pereira, *J. Coat. Technol. Res.*, 12 (2015) 1.
2. N. Wang, Y.N. Zhang, J.S. Chen, J. Zhang and Q.H. Fang, *Prog. Org. Coat.*, 109 (2017) 126.
3. H.H. Zhang, R. Niu, X.B. Guan, D.H. Xu and T.F. Shi, *Chin. J. Polym. Sci.*, 33 (2015) 1750.
4. J.O. Akindoyo, M.D.H. Beg, S. Ghazali, M.R. Islam, N. Jeyaratnam and A.R. Yuvaraj, *Rsc. Adv.*, 6 (2016) 114453.
5. A. Noreen, K.M. Zia, M. Zuber, S. Tabasum and M.J. Saif, *Korean. J. Chem. Eng.*, 33 (2016) 388.
6. F.G. Liu, A.M. Liu, W.J. Tao and Y.J. Yang, *Prog. Org. Coat.*, 145 (2020) 105685.
7. Q.F. Mo, W.Z. Li, H.J. Yang, F.M. Gu, Q.Z. Chen and R.X. Yang, *Prog. Org. Coat.*, 136 (2019) 105213.
8. J. Li, J.C. Cui, J.Y. Yang, Y.Y. Li, H.X. Qiu and J.H. Yang, *Compos. Sci. Technol.*, 129 (2016) 30.
9. G. Cui, Z.X. Bi, R.Y. Zhang, J.G. Liu, X. Yu and Z.L. Li, *Chem. Eng. J.*, 373 (2019) 104.
10. L. Gu, J.H. Ding and H.B. Yu, *Prog. Chem.*, 28 (2016) 737.
11. C.L. Zhang, X.Y. Dai, Y.N. Wang, G.E. Sun, P.H. Li, L.J. Qu, Y.L. Sui and Y.L. Dou, *Coatings.*, 9 (2019) 46.
12. J.C. Cui, J.C. Xu, J. Li, H.X. Qiu, S.Y. Zheng and J.H. Yang, *Compos. Pt. B-Eng.*, 188 (2020) 107889.
13. A. Bouibed and R. Doufnoune, *J. Adhes. Sci. Technol.*, 33 (2019) 834.
14. L. Guo, *Int. J. Electrochem. Sci.*, 13 (2018) 11867.
15. Y.Z. Xia, H. Cheng, L.J. Duo, D. Zhang, X.N. Chen, S.X. Shi and L. Lei, *J. Appl. Polym. Sci.*, 137 (2019) 48733.
16. Z.X. Yu, H.H. Di, Y. Ma, L. Lv, Y. Pan, C.L. Zhang and Y. He, *Appl. Surf. Sci.*, 351 (2015) 986.
17. H.H. Di, Z.X. Yu, Y. Ma, Y. Pan, H. Shi, L. Lv, F. Li, C. Wang, T. Long and Y. He, *Polym. Adv. Technol.*, 27 (2016) 915.
18. H.H. Di, Z.X. Yu, Y. Ma, F. Li, L. Lv, Y. Pan, Y. Lin and Y. Liu, *J. Taiwan Inst. Chem. Eng.*, 64 (2016) 244.
19. X. Wang, *Int. J. Electrochem. Sci.*, 15 (2020) 1450.

20. S. Pazokifard, M. Esfandeh and S.M. Mirabedini, *Prog. Org. Coat.*, 77 (2014) 1325.
21. E. Aliyev, V. Filiz, M.M. Khan, Y.J. Lee, C. Abetz and V. Abetz, *Nanomaterials.*, 9 (2019) 1180.
22. P. Bhawal, S. Ganguly, T.K. Chaki and N.C. Das, *Rsc. Adv.*, 6 (2016) 20781.
23. X.L. Liu, X.B. Zou, Z. Ge, W.G. Zhang and Y.J. Luo, *Rsc. Adv.*, 9 (2019) 31357.
24. Y.L. Zhang, L.S. Shao, D.Y. Dong and Y.H. Wang, *Rsc. Adv.*, 6 (2016) 17163.
25. M.B. Kale, Z. Luo, X. Zhang, D. Dhamodharan, N. Divakaran, S. Mubarak, L.X. Wu and Y. Xu, *Polymer.*, 170 (2019) 43.
26. K.W. Cai, S.X. Zuo, S.P. Luo, C. Yao, W.J. Liu, J.F. Ma, H.H. Mao and Z.Y. Li, *Rsc. Adv.*, 6 (2016) 95965.
27. Y.T. Wu, S.G. Wen, K.M. Chen, J.H. Wang, G.Y. Wang and K. Sun, *Prog. Org. Coat.*, 132 (2019) 409.
28. Z.H. Zhao, L. Guo, L. Feng, H. Lu, Y. Xu, J.N. Wang, B. Xiang and X.F. Zou, *Eur. Polym. J.*, 120 (2019) 109249.
29. K. Rajtha, K.N.S. Mohana, A. Mohanan and A.M. Madhusudhana, *Colloid Surf. A-Physicochem. Eng. Asp.*, 587 (2020) 124341.
30. F.Y. Zhang, W.Q. Liu, L.Y. Liang, S. Wang, H.Y. Shi, Y.K. Xie, M.P. Yang and K. Pi, *Colloid Surf. A-Physicochem. Eng. Asp.*, 591(2020) 124565.
31. N. Parhizkar, T. Shahrabi and B. Ramezanzadeh, *Corros. Sci.*, 123 (2017) 55.
32. B. Ramezanzadeh, Z. Haeri and M. Ramezanzadeh, *Chem. Eng. J.*, 303 (2016) 511.

© 2020 The Authors. Published by ESG ([www.electrochemsci.org](http://www.electrochemsci.org)). This article is an open access article distributed under the terms and conditions of the Creative Commons Attribution license (<http://creativecommons.org/licenses/by/4.0/>).